Transition rates between two-body states in ^{206}Tl, ^{208}Bi, and ^{210}Bi

D. J. Donahue,* O. Häusser,† R. L. Hershberger, R. Lutter, and F. Riess
Sektion Physik der Universität München, München, Germany
(Received 30 June 1975)

Recoil-distance techniques have been used to measure mean lives of some two-hole, particle-hole, and two-particle states in ^{206}Tl, ^{208}Bi, and ^{210}Bi. A comprehensive comparison is presented of these results and all other known $E2$ and $M1$ matrix elements for two-body states with calculations. The calculations are made using wave functions of Ma and True and of Kuo and Herling together with known effective single-particle matrix elements. Reasonable agreement is obtained, particularly with the Kuo-Herling wave functions. From measurements of the $1^- \rightarrow 0^-$ $M1$ transition rate in ^{206}Tl, the magnetic moment of the $3s_{1/2}$ proton-hole state in ^{207}Tl is determined to be $\mu = (1.83 \pm 0.18)\mu_N$.

[NUCLEAR REACTIONS ^{205}Tl(^{17}O, ^{16}O), ^{209}Bi(^{17}O, ^{18}O), and ^{209}Bi(^{17}O, ^{16}O) at 75 MeV. Recoil-distance Doppler-shift measurements used to deduce $T_{1/2}$ of states in product nuclei.]

I. INTRODUCTION

In recent years several systematic studies of electromagnetic properties for nuclear states near the ^{208}Pb doubly-closed shell have appeared.[1-6] At present about 13 $M1$ and 10 $E2$ matrix elements for single particle states are known experimentally and are reasonably well accounted for by calculation of renormalized "effective" g factors[1-3] and charges.[4-6] Of special importance for the measurement of single particle matrix elements (SPME) has been the existence of essentially pure two-component states of high spin and long half-life. The isomerism of these states is a result of the energy splitting of multiplets by the effective nucleon-nucleon interaction. The SPME are deduced from the measured half-lives and g factors using "additivity" relationships of the nuclear shell model.

On the other hand, there is little information on transition rates for the shorter lived ($\tau < 1$ ns) two-component states near ^{208}Pb although the majority of states have half-lives in the subnanosecond region. The only study reported, by Olin *et al.*[7] for ^{208}Bi, made use of the ^{207}Pb(^{7}Li, $\alpha 2n\gamma$)^{208}Bi reaction together with the Doppler-shift attenuation method.

In the present work we have measured lifetimes of two-component states in ^{206}Tl, ^{208}Bi, and ^{210}Bi by the recoil-distance method. The states were populated by the (^{17}O, ^{16}O) and the (^{17}O, ^{18}O) heavy-ion transfer reactions to impart sufficiently large velocities to the recoiling nuclei. Several $M1$ and $E2$ transition matrix elements were deduced from the measured lifetimes and are compared to theoretical estimates based on the work of Kuo and Herling[8] and of Ma and True.[9] The authors use different effective nucleon-nucleon interactions which generate energy splittings in good agreement with the observed energy spectra in nuclei with masses 206, 208, and 210. These comparisons have been extended to all known $M1$ and $E2$ matrix elements for two-component states, and provide an extremely sensitive test of the wave functions and of the effective SPME used in the calculation.

For one of the transitions studied here, the 305-keV transition between the two $(s_{1/2}p_{1/2})$ states in ^{206}Tl, an estimate is obtained for the $3s_{1/2}$ proton-hole magnetic moment.

II. EXPERIMENTAL PROCEDURE

Excited states in ^{206}Tl, ^{208}Bi, and ^{210}Bi from the reactions ^{205}Tl(^{17}O, ^{16}O)^{206}Tl, ^{209}Bi(^{17}O, ^{18}O)^{208}Bi, and ^{209}Bi(^{17}O, ^{16}O)^{210}Bi, were produced by bombarding targets of ^{205}Tl and ^{209}Bi with 75-MeV ^{17}O ions from the München MP tandem accelerator. The targets were made by evaporating approximately 1 mg/cm^2 of ^{205}Tl and bismuth onto stretched aluminum foils which were 0.15 mg/cm^2 thick. Deexcitation γ rays were detected at 0° in a germanium diode with a volume of about 70 cm^3, and those γ-ray pulses in coincidence with backscattered particles were analyzed and stored together with the particle pulses in a PDP-10 computer. The arrangement of target and stopper was such that the ^{17}O beam passed first through the ^{205}Tl or ^{209}Bi target, then through the aluminum foil, and finally through a stretched 3-mg/cm^2 Au stopper. The beam was stopped about 4 cm from the target-stopper assembly by thick bismuth. With this arrangement, oxygen ions backscattered from the ^{205}Tl and ^{209}Bi could be resolved in energy from those scattered by the thicker Au stopper. By using an appropriate window in the particle spectrum, γ rays from gold could be nearly completely

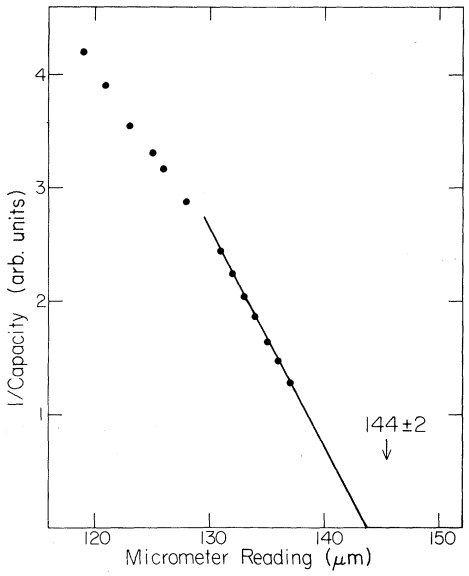

FIG. 1. The reciprocal of the capacitance of the target-stopper assembly plotted, in arbitrary units, as a function of the setting of the micrometer on the plunger apparatus. The difference between the intercept of the curve and the micrometer reading at a particular setting is the target-stopper separation D at that setting.

eliminated from the γ-ray spectrum.

The plunger apparatus and target construction used in these experiments were similar to those used at Chalk River, which have been described in detail elsewhere.[10] An important feature of the design is the fact that the target and stopper form a parallel-plate capacitor whose capacitance is accurately inversely proportional to the separation of the target and stopper. Figure 1 shows a plot of the reciprocal of this capacitance vs target-stopper separation obtained in beam with a ^{205}Tl target and a stretched gold foil stopper. As can be seen from the curve, we were able to take data at a separation of 8 μm. In addition, a linear extrapolation of the curve shown in Fig. 1 enabled us to determine the position of zero separation of the target and stopper to an accuracy of 2 μm. As will be seen, this accurate knowledge of the position of zero separation proved to be very important in the measurements of short-lived states, expecially when such states were only weakly excited by the transfer reactions used in this work. The capacitance of the target-stopper system was monitored continuously, and its instantaneous value was stored with each particle-γ-ray coincidence. For γ rays from a particular state, spectra from the germanium detector obtained at each target-stopper separation, D, were fitted to a functional form of two Gaussian peaks superimposed on a linear or quadratic background. The positions and widths of the Gaussian peaks were determined from an analysis of a sum of the data collected at all target-stopper separations. The recoil velocity was, on the average, $v=[(1.06\pm0.03)\%]c$, and, for all transitions analyzed, the separation between stopped and shifted peaks exceeded the detector resolution (~2.5 keV for 1.33-MeV γ rays). The ratio $R=I_0/(I_0+I_s)$, where I_0 is the area of the stopped peak and I_s is the area of the shifted peak, was obtained for each value of D, and a plot of R vs D was fitted to obtain the mean life of the state under study. The computer program used to obtain these fits could be made to include cascades from higher states. Such cascade corrections will be discussed for individual cases below.

Since the yield of the transfer reactions was usually small, statistical uncertainties limited the precision with which mean lives could be measured to between 10 and 30%. Therefore, no corrections were made to the data for second-order effects.

III. RESULTS

A. States in thallium

Figure 2 shows a spectrum of γ rays in coincidence with backscattered ions resulting from the bombardment of a ^{205}Tl target with 75-MeV ^{17}O ions. This spectrum was obtained with a detector located at 90° to the direction of recoiling thallium nuclei, and is a sum of all the data accumulated in a period of about 40 h with a beam of about 30 nA of 7^+ ^{17}O ions. Measurements made on individual γ rays are described below and the results are listed in Table I. The column in the table labeled R_∞ indicates the magnitude of the ratio $R=I_0/(I_0+I_s)$ at very large values of the target-stopper separation. These long-lived backgrounds presumably result from cascades from very long-lived states.

1. 305-keV (1^-) state

The 305-keV γ rays seen in Fig. 2 are from transitions between the 305-keV (1^-) and the (0^-) ground state. Since both of these states have predominant configurations of $(\pi s_{1/2})(\nu p_{1/2})$, the $M1$ transition rate between them is directly related to the $3s_{1/2}$ single-proton magnetic moment, and is of particular interest. However, the determination of the mean life of the 305-keV state is complicated by the fact that it is fed by cascades from the 635-keV state, as indicated by the presence of 330-keV γ rays in Feg. 2. In addition, there is a very long-lived component present in the stopped peak. Figure 3 shows a plot of the quantity $R=I_0/(I_0+I_s)$ as a function of the target-

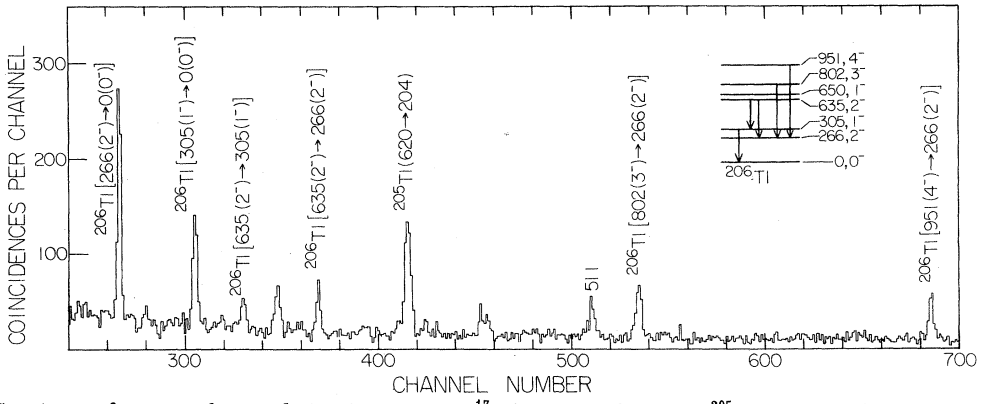

FIG. 2. Spectrum of γ rays observed at 90° to 75-MeV ^{17}O beam incident on a ^{205}Tl target. This spectrum is the sum of spectra collected at all observed target-stopper separations. The energy dispersion of the system is about 1 keV/channel.

stopper separation distance D. In this plot a constant background with the magnitude indicated in Table I has already been subtracted. The data shown in Fig. 3 were fitted with a computer-calculated curve in which the fraction of the feeding from the 635-MeV state, the mean life of that state, and the zero position of the target-stopper separation obtained from Fig. 1 were known inputs. The fraction of the feeding from the 635-keV state was obtained from the data illustrated in Fig. 2, and the determination of the mean life of this state is described below. The value of the mean life of the 305-keV state was then adjusted to give the best fit to the data. Because of the uncertainties in the properties of the 635-keV state and because of the poor statistical precision of the data, the mean life of the 305-keV state could be determined with a precision of only 33%.

2. 635-keV (2^-) state

Figure 4 shows a plot of R vs D for this state. The data shown in the figure represent a sum of the intensities of the 330- and 369-keV γ rays emitted as this state decays to the 305-keV (1^-) and 266-keV(2^-) states. No correction for cascades from short-lived states was necessary, and the data were analyzed to yield values for the mean life of the 635-keV state and the long-lived background component R_∞. This background has been subtracted from the data illustrated in Fig. 4.

3. 802-keV (3^-) and 951-keV (4^-) states

Plots of R vs D for these two states are shown in Figs. 5 and 6. The 802-keV state decays by emission of 536-keV γ rays to the 266-keV (2^-) state. It has a relatively short mean life, and only an accurate knowledge of the zero-separation point allows a determination of this mean life.

The 685-keV γ rays emitted in the 951-keV (4^-) to 266-keV (2^-) transition were used to determine the mean life of the 951-keV state. The solid curve in Fig. 6 is a fit to the data in which the amount of long-lived background R_∞ was considered as one of the variables.

TABLE I. Experimental results.

Nucleus	Initial state, energy (keV) Principal configuration (π, ν)	Final state	R_0	τ (ps)
^{206}Tl	$1^-(305)s_{1/2}p_{1/2}$	$0^-(0)s_{1/2}p_{1/2}$	0.25 ± 0.04	6.1 ± 2.0
^{206}Tl	$2^-(635)s_{1/2}p_{3/2}$	$2^-(266)s_{1/2}f_{5/2}+d_{3/2}p_{1/2}$	0.24 ± 0.04	5.8 ± 1.3
^{206}Tl	$2^-(635)s_{1/2}p_{3/2}$	$1^-(305)s_{1/2}p_{1/2}$		
^{206}Tl	$3^-(802)s_{1/2}f_{5/2}$	$2^-(266)s_{1/2}f_{5/2}+d_{3/2}p_{1/2}$	...	3.5 ± 1.0
^{206}Tl	$4^-(951)d_{3/2}f_{5/2}$	$2^-(266)s_{1/2}f_{5/2}+d_{3/2}p_{1/2}$	0.1 ± 0.1	60 ± 15
^{208}Bi	$6^+(510)h_{9/2}f_{5/2}^{-1}$	$5^+(0)h_{9/2}p_{1/2}^{-1}$	0.32 ± 0.03	170 ± 20
^{208}Bi	$4^+(601)h_{9/2}f_{5/2}^{-1}$	$5^+(0)h_{9/2}p_{1/2}^{-1}$	0.28 ± 0.06	8 ± 3
^{210}Bi	$2^-(319)h_{9/2}g_{9/2}$	$1^-(0)h_{9/2}g_{9/2}$	0.15 ± 0.03	7.5 ± 1.5
^{210}Bi	$8^-(582)h_{9/2}g_{9/2}$	$9^-(271)h_{9/2}g_{9/2}$	0.17 ± 0.03	< 2.5
^{210}Bi	$10^-(669)h_{9/2}i_{11/2}$	$9^-(271)h_{9/2}g_{9/2}$	0.13 ± 0.06	144 ± 25

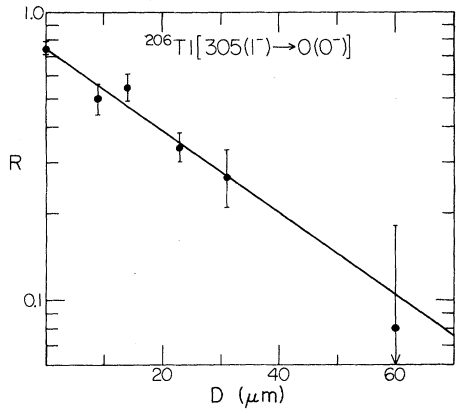

FIG. 3. A decay curve for the 305-keV state in ^{206}Tl. The ratio $R = I_0/(I_0 + I_s)$ is plotted on a logarithmic scale as a function of the target-stopper distance D. In the ratio R, I_0 is the area of the stopped peak and I_s is the area of the shifted peak. A constant background R_∞ has been subtracted from each point.

B. States in ^{208}Bi and ^{210}Bi

Figure 7 shows a spectrum of γ rays in coincidence with backscattered particles from a bismuth target. As in Fig. 2, this spectrum was collected with a Ge(Li) detector placed at 90° to the incident beam and recoil direction, and is a sum of data taken at six target-stopper separations. The time of accumulation for this spectrum was about 50 h, and the beam was about 20 nA of 7^+ ^{17}O.

γ rays from only two of the ten lowest excited states in ^{210}Bi are seen with any appreciable intensity. These are the 398-keV γ rays from the 669-keV (10^-)→271-keV (9^-) transition, and the 311-keV γ rays from the 582-keV (8^-)→271-keV (9^-) transition. Most of the other low-lying states in ^{210}Bi decay with the emission of γ rays with

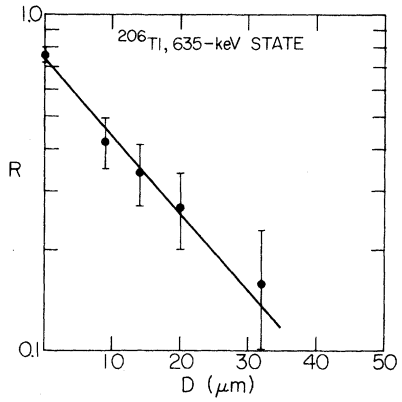

FIG. 4. A plot of the ratio R, on a logarithmic scale vs D for the decay of the 635-keV state in ^{206}Tl. Definitions of R and D are given in the caption of Fig. 3. A constant background R_∞ has been subtracted from each point.

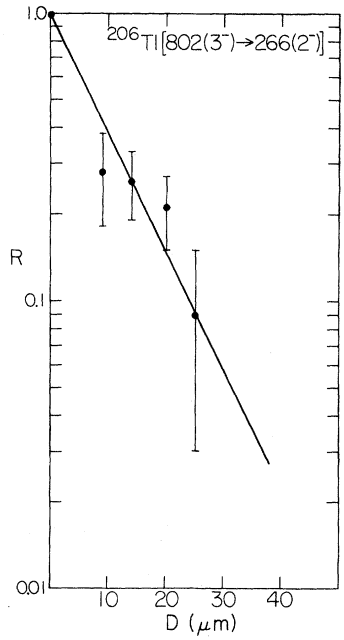

FIG. 5. A plot of the ratio R, on a logarithmic scale, as a function of target-stopper separation D for the decay of the 802-keV state in ^{206}Tl.

energies less than about 200 keV. The electronics used in these experiments strongly discriminated against γ-ray energies less than 200 keV.

Plots of R vs D obtained for the 398-keV and 311-keV γ rays from ^{210}Bi are shown in Figs. 8 and 9, respectively. The solid curve in Fig. 8 is a computer fit to the experimental data. In this calculation, the value of R_∞ was considered variable. In the results presented in Fig. 9 for the 311-keV transition, a measured value of R_∞ has been subtracted. Only an accurate knowledge of the zero-

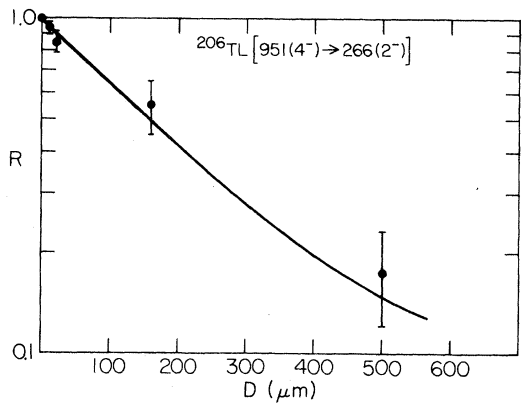

FIG. 6. A decay curve for the 951-keV state in ^{206}Tl. The ratio R is plotted, on a logarithmic scale, as a function of the target-stopper separation D. The solid curve is fitted to the data and includes a single decay curve and a constant background.

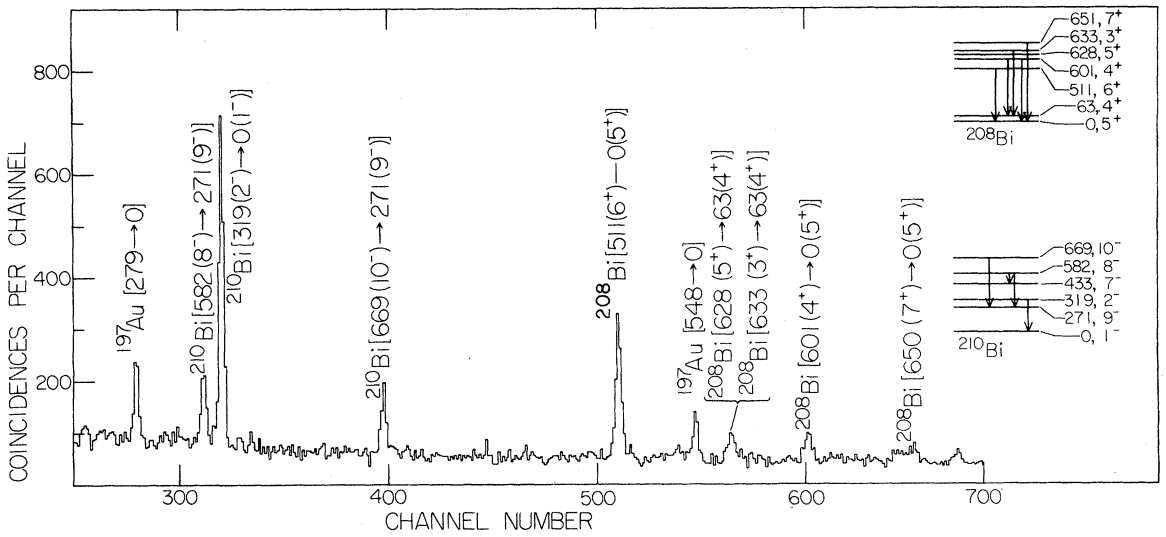

FIG. 7. Spectrum of γ rays observed at 90° to a 75-MeV ^{17}O beam incident on a ^{209}Bi target. This spectrum is the sum of spectra collected at several observed target-stopper separations. The energy dispersion is about 1 keV/channel.

separation point of the target and stopper makes possible a determination of the mean life of the 582-keV state.

In contrast to the case for ^{210}Bi, γ rays can be seen in Fig. 7 from all of the low-lying states in ^{208}Bi which have as their predominant configuration $(\pi h_{9/2})(\nu f_{5/2}^{-1})$. These states are formed by stripping an $f_{5/2}$ neutron from ^{209}Bi, and the yields of γ rays shown in Fig. 7 indicate that they are all produced with comparable intensities. However, only the mean life of the 510-keV (6^+) state could be deduced from our results. γ rays from the 628-keV (5^+) and 633-keV (3^+) states with energies of 565 and 570 keV, respectively, could not be resolved, and those from the 661-keV (4^+) and the 651-keV (7^+) states were too weak to be analyzed.

Results for the 510-keV γ rays emitted in the 510-keV (6^+)→0-keV (4^+) transition are shown in Figs. 10 (a) and 10 (b). As can be seen from Fig. 10 (a), the spectrum contains a large long-lived unshifted component. The intensity of this long-lived component is consistent with the supposition that it results from the cascade decay of the 651-keV state through the 510-keV state. The

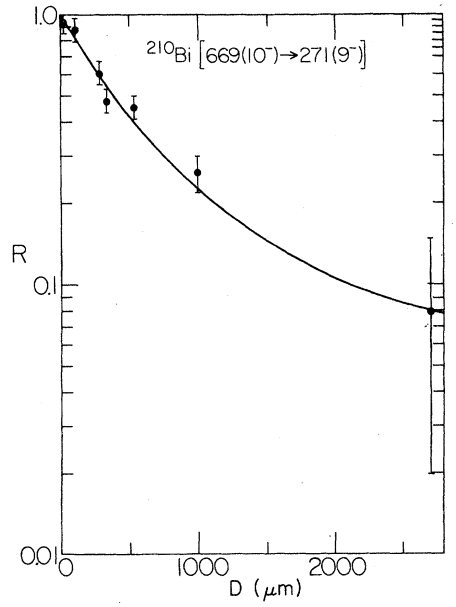

FIG. 8. A plot of the ratio R, on a logarithmic scale, vs target-stopper separation D obtained for 398-keV γ rays from the 669-keV state in ^{210}Bi. The solid curve is a best fit to the experimental points.

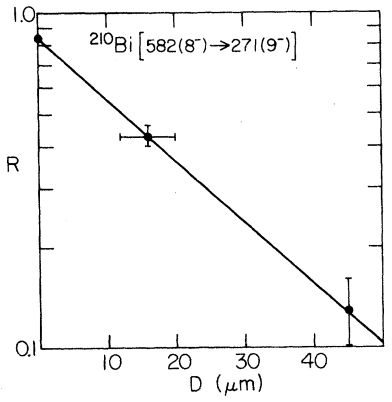

FIG. 9. A plot of the ratio R, on a logarithmic scale, as a function of target-stopper separation D obtained for the 311-keV γ rays from the 582-keV state in ^{210}Bi. A constant background, R_∞, has been subtracted from each point.

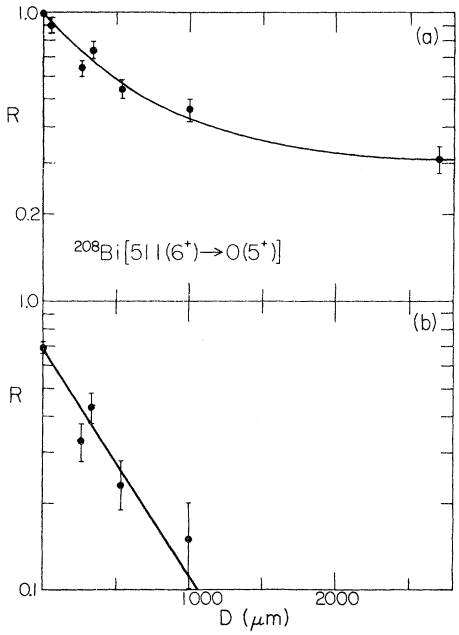

FIG. 10. The ratio R vs target-stopper distance D for the decay of the 510-keV state in ^{208}Bi. The data in (a) include a long-lived background, and the solid curve is a fit to these data. In part (b) the long-lived component has been subtracted.

141-keV γ rays emitted in the cascade transition are strongly converted, and in addition, as mentioned above, could not be detected in this experiment. If, indeed, the long-lived component comes from the 651-keV state, a limit to the mean life of that state of $\tau > 1.5$ ns can be given. Because of the behavior of the 510-keV peak as a function of the width and position of the window used in the particle spectrum, we conclude that not more than 6% of the 510-keV γ rays arose from annihilation radiation.

IV. COMPARISON OF EXPERIMENTAL AND THEORETICAL TWO-BODY MATRIX ELEMENTS

All experimentally known magnetic moments, quadrupole moments, $B(M1)$, and $B(E2)$ values for two-component states near ^{208}Pb have been collected in Tables II–IV. The data take calculated internal conversion coefficients and experimental branching ratios into account. For comparison theoretical predictions are also shown, using either pure configurations or the full wave functions of Kuo and Herling[8] or of Ma and True.[9] The two-component matrix elements were deduced using the formula

$$\langle j_1 j_2 j \,\|T^k\|\, j_1' j_2' j' \rangle = (-)^{j_1'-j_2+j-k}(2j+1)^{1/2}(2j'+1)^{1/2} W(j_1 j j_1' j'; j_2 k)\langle j_1 \|T^k\| j_1'\rangle \delta_{j_2 j_2'} + (-)^{j_2-j_1'+j'-k}(2j+1)^{1/2}(2j'+1)^{1/2} W(j_2 j j_2' j'; j_1 k)\langle j_2 \|T^k\| j_2'\rangle \delta_{j_1 j_1'} .$$

The single-particle matrix elements $\langle j \|T^k\| j' \rangle$ have been taken from experiment or from theoretical estimates as indicated in Table V. Great care has been taken to ensure that the coupling of spin and angular momentum and the definition of radial wave functions agree with Refs. 8 and 9. It was also essential to take the change of sign for $E2$ matrix elements into account when going from single-particle to single-hole states. The calculations were performed using a computer program. The correctness of the program was verified by exactly reproducing the calculations of $M1$ and $E2$ transition rates for states in ^{206}Pb by True and Ford.[29]

The matrix elements are related to magnetic moments, static quadrupole moments, and reduced transition probabilities by the following formulas:

$$Q_I = \left(\frac{16\pi}{5}\right)^{1/2}\left(\frac{2I(2I-1)}{(2I+3)(2I+2)(2I+1)}\right)^{1/2}\langle I\|E2\|I\rangle ,$$

$$\mu_I = \left(\frac{4\pi}{3}\right)^{1/2}\left(\frac{2I}{(2I+2)(2I+1)}\right)^{1/2}\langle I\|M1\|I\rangle ,$$

$$B(M1; I \to I') = \frac{|\langle I\|M1\|I'\rangle|^2}{2I+1},$$

$$B(E2; I \to I') = \frac{|\langle I\|E2\|I'\rangle|^2}{2I+1}.$$

To deduce matrix elements from measured transition rates, it is necessary to know multipole mixing ratios. In all cases where mixed transitions are possible, multipole mixing ratios were calculated using both sets of wave functions. The calculations show that where $M1$ and $E2$ mixtures are allowed almost all of the transitions studied were overwhelmingly $M1$. However, for the $6^+ \to 5^+$ transition in ^{208}Bi, $M1$ matrix elements effectively cancel and the transition is predominantly $E2$. Branching ratios used in the calculations were taken from the work of Proetel *et al.*[30, 31] for ^{208}Bi and ^{210}Bi, and from the Nuclear Data Sheets[12] for ^{206}Tl.

V. DISCUSSION

The over-all agreement between the calculated and experimental electromagnetic properties of

TABLE II. Moments of two-particle states.

Nucleus	E_x (keV)	J^π	Pure conf.	Kuo-Herling	Ma-True	μ_{exp} (μ_N)	Reference
			Magnetic moments (μ_N)				
^{206}Pb	2200	7^-	−0.41	−0.13	−0.18	−0.152 ± 0.003	11
	2384	6^-	−1.49	−1.59	−1.54	0.78 ± 0.42	12
	4027	12^+	−1.85	−1.85	−1.85	−1.86 ± 0.05	13
^{208}Bi	1571	10^-	2.61	2.61	3.20	2.666 ± 0.027	14
^{210}Bi	0	1^-	0.31	0.04	−0.86	−0.044 ± 0.0001	15
	433.1	7^-	2.14	2.16	2.12	2.11 ± 0.05	16
	438.9	5^-	1.53	1.54	1.50	1.53 ± 0.05	16
^{210}Po	1472	6^+	5.44	5.45	5.45	5.58 ± 0.12	17
	1552	8^+	7.25	7.27	7.31	7.28 ± 0.08	17
			Quadrupole moments (e fm^2)				
^{206}Pb	803.1	2^+	16	28	28	25 ± 15	18
^{210}Bi	0	1^-	18	15	7	13 ± 1	15

two-body states near ^{208}Pb is relatively impressive. It gives credence to both the single-particle matrix elements of Table V and to the two-body matrix elements used to calculate the configuration mixing, particularly those of Kuo and Herling.[8] Several observations can be made after a closer inspection of Tables II–IV.

(1) For magnetic dipole moments agreement between theory and experiment is good. In most cases, calculated and experimental numbers are within a few percent of one another. An obvious exception is provided by the 6^- state in ^{206}Pb, where the moments disagree even in sign, causing some doubt on the identification of the 2384-keV state.

(2) Of the 16 $M1$ transition rates listed in Table III, all but three are within a factor of 2 of calculated rates, and half of them agree with calculations within experimental error. The two transitions from the 1033-keV state in ^{208}Bi are very slow, and according to Olin *et al.*,[7] calculations could be made to agree with experiment if this state included a 10% admixture of $(1h_{9/2})(3p_{3/2})^{-1}$. The reason for the large disagreement for the $2^- \rightarrow 1^-$, 319-keV transition in ^{210}Bi is not clear. It is possible that an unobserved cascade caused us to measure a mean life that was too long.

Almost all of the measured transition rates of Olin *et al.*[7] in ^{208}Bi are systematically smaller than calculated rates, and a small change in slowing down powers used to interpret their Doppler-shift measurements would improve the agreement.

(3) The $B(E2)$ values of Table IV show better agreement for the Kuo-Herling wave functions and indicate that configuration mixing in the Ma-True wave functions is too large. The experimental $B(E2)$ values for the $4^- \rightarrow 2^-$ transition in ^{206}Tl and the $4^+ \rightarrow 2^+$ transition in ^{210}Pb disagree with both calculations.

(4) The 305-keV, $1^- \rightarrow 0^-$ transition in ^{206}Tl is predominantly a $(\pi 3s_{1/2})(\nu 3p_{1/2}) \rightarrow (\pi 3s_{1/2})(\nu 3p_{1/2})$ transition. The $M1$ matrix element for this transition can be written in terms of single-particle magnetic moments as

$$\langle f \| M1 \| i \rangle = \frac{3}{\sqrt{4\pi}} [\mu(s_{1/2}) - \mu(p_{1/2})] .$$

Using our measured value for $B(M1)$ $1^- \rightarrow 0^-$ in ^{206}Tl, a value of $\mu(p_{1/2}) = 0.59$, we obtain the result

$$\mu(s_{1/2}) = 1.83 \pm 0.18 .$$

The error includes uncertainties in the configuration mixing estimated from the difference in the wave functions in Refs. 8 and 9. The deduced magnetic moment is strongly reduced from the single-particle value $\mu = 2.793$, and is found in good agreement with the theoretical estimate $\mu(^{207}\text{Tl}, s_{1/2}) = 1.935\mu_N$, by Bauer *et al.*,[2] which is based on the theory of finite Fermi systems. Because of the vanishing orbital angular momentum, mesonic contributions are expected to be small and the observed deviation from the Schmidt value is therefore almost entirely attributable to core polarization.

The result obtained is somewhat larger than the

TABLE III. $M1$ transitions between two-particle states.

Nucleus	E_i (keV)	$J_i^\pi \to J_f^\pi$	E_γ (keV)	Pure conf.	Kuo-Herling	Ma-True	$B(M1)_{exp}$ (μ_N^2)	Reference
^{206}Tl	305	$1_1^- \to 0_1^-$	305	0.435	0.310	0.284	0.24 ±0.08	Present work
	635	$2_2^- \to 1_1^-$	330	0.409	0.074	0.081	0.11 ±0.02	Present work
		$2_2^- \to 2_1^-$	369	0	0.036	2×10^{-5}	0.077±0.017	Present work
	801.6	$3_1^- \to 2_1^-$	536	0	0.071	0.33	0.10 ±0.03	Present work
	951	$4_1^- \to 3_1^-$	149	0.023	0.017	0.021	0.036±0.009	Present work
^{206}Pb	2384	$6_1^- \to 7_1^-$	184	0.23	0.14	0.16	0.075±0.024	12
^{207}Bi	886	$5_3^+ \to 4_1^+$	823	0.16	0.32	0.24	0.18 ±0.07	7
		$5_3^+ \to 5_1^+$	886	0.25	0.29	0.33	0.15 ±0.06	7
	1033	$4_4^+ \to 4_1^+$	970	0.0001	0.0001 [a]	0.001 [a]	0.17 ±0.005	7
		$4_4^+ \to 5_1^+$	1033	0.004	0.004 [a]	0.006 [a]	0.035±0.010	7
^{208}Bi	1069	$3_3^+ \to 4_2^+$	468	0.008	0.16	0.20	0.13 ±0.05	7
		$3_3^+ \to 4_1^+$	1007	0.41	0.14	0.17	0.070±0.025	7
	1095	$6_2^+ \to 5_3^+$	208	0.83	0.88	0.89	0.64 ±0.32	7
		$6_2^+ \to 5_1^+$	1095	0.41	0.36	0.30	0.21 ±0.07	7
^{210}Bi	319	$2_1^- \to 1_1^-$	319	3.31	2.96	1.58	0.16 ±0.03	Present work
	699	$10_1^- \to 9_1^-$	398	0.010	0.014	0.007	0.005±0.001	Present work

[a] Reference 7 claims that a 10% admixture of $(1h_{9/2})(3p_{3/2})^{-1}$ in the 4_4^+ state will give agreement with experiment.

TABLE IV. $E2$ transitions between two-particle states.

	E_i (keV)	$J_i \to J_f$	E_γ (keV)	Pure conf.	Kuo-Herling	Ma-True	$B(E2)_{exp}$ (e^2 fm^4)	Reference
^{206}Tl	255	$2_1^- \to 0_1^-$	266	112	134	165	123	12
	951	$4_1^- \to 2_1^-$	685	71	243	326	46 ±12	Present work
^{206}Pb	803	$2_1^+ \to 0_1^+$	803	85	190	183	184 ±10	12
	4027	$12^+ \to 10^+$	69.6	(24)	(24)	(24)	24 ±2	12
^{208}Bi	510	$6_1^+ \to 5_1^+$	510	51	89	114	137 ±20	Present work
	936	$3_2^+ \to 5_1^+$	936	1.7	5	0.3	7.8	7
^{210}Pb	1091	$4_1^+ \to 2_1^+$	296	141	156	150	367 ±61	19
^{210}Bi	433	$7_1^- \to 9_1^-$	162	25	42	68	43 ±1	19
	439	$5_1^- \to 3_1^-$	91.3	164	176	159	173 ±5	19
^{210}Po	1426	$4_1^+ \to 2^+$	245	242	269	231	285 ±32	19
	1472	$6_1^+ \to 4_1^+$	46.5	167	182	161	247 ±33	19
	1552	$8_1^+ \to 6_1^+$	83.7	67	66	65	73 ±6	19

TABLE V. Single-particle matrix elements.

Initial state	Final state	$\langle f\|M1\|i\rangle$ (μ_N)	Reference	$\langle f\|E2\|i\rangle$ (e fm^2)	Reference
			Proton		
$3s_{1/2}$	$3s_{1/2}$	2.32	20		
$2d_{3/2}$	$3s_{1/2}$	−0.30	20	−33.5	21
$2d_{5/2}$	$3s_{1/2}$			37.1	5
$2d_{3/2}$	$2d_{3/2}$	0.96	20	29.6	5
$2d_{5/2}$	$2d_{3/2}$	−1.90	20	20.5	5
$1g_{7/2}$	$2d_{3/2}$			35.8	5
$2d_{5/2}$	$2d_{5/2}$	5.93	20	40.1	5
$1g_{7/2}$	$1g_{7/2}$	4.69	20	43.1	5
$1h_{11/2}$	$1h_{11/2}$	12.71	20	74.5	5
$1h_{9/2}$	$1h_{9/2}$	6.97	23	−51.3	22
$2f_{7/2}$	$1h_{9/2}$	0.18	22, 6	−15.5	6
$2f_{5/2}$	$1h_{9/2}$			−62.9	5
$2f_{7/2}$	$2f_{7/2}$	8.41	20	−53.5	5
$2f_{5/2}$	$2f_{7/2}$	2.14	6	19.9	5, 6
$3p_{3/2}$	$2f_{7/2}$			−54.4	5
$2f_{5/2}$	$2f_{5/2}$	2.42	20	−46.5	5
$3p_{3/2}$	$2f_{5/2}$			−20	5
$3p_{1/2}$	$2f_{5/2}$			−38.7	5
$1i_{13/2}$	$1i_{13/2}$	15.71	23	−90.7	5
$3p_{3/2}$	$3p_{3/2}$	3.95	20	−32.4	5
$3p_{1/2}$	$3p_{3/2}$	1.51	20	33.2	5
$3p_{1/2}$	$3p_{1/2}$	−0.10	20		
			Neutron		
$3p_{1/2}$	$3p_{1/2}$	0.71	23		
$3p_{3/2}$	$3p_{1/2}$	1.28	6	15.6	6
$2f_{5/2}$	$3p_{1/2}$			20.6	
$3p_{3/2}$	$3p_{3/2}$	−1.60	20, 3	16.9	5
$2f_{5/2}$	$3p_{3/2}$	−0.44	24	−11.2	5, 6
$2f_{7/2}$	$3p_{3/2}$			27.7	5, 6
$2f_{5/2}$	$2f_{5/2}$	1.08	23	25.9	5
$2f_{7/2}$	$2f_{5/2}$	1.98	6	11.7	5, 6
$2f_{7/2}$	$2f_{7/2}$	−2.01	20, 3	48.5	28
$1i_{13/2}$	$1i_{13/2}$	−1.96	23	54.2	5
$1h_{9/2}$	$1h_{9/2}$	1.18	20	31.1	5
$2g_{9/2}$	$2g_{9/2}$	−2.27	23	−39.2	27
$1i_{11/2}$	$2g_{9/2}$	0.35	25	6.9	5, 6
$3d_{5/2}$	$2g_{9/2}$			−32.9	6
$2g_{7/2}$	$2g_{9/2}$	−1.96	20	11.7	5, 6
$1i_{11/2}$	$1i_{11/2}$	1.07	20	−39.3	5
$2g_{7/2}$	$1i_{11/2}$		20	−40.0	5, 6
$1j_{15/2}$	$1j_{15/2}$	−2.68	20	−64.0	5
$3d_{5/2}$	$3d_{5/2}$	−1.90		−18.1	5
$4s_{1/2}$	$3d_{5/2}$			−17.7	26
$2g_{7/2}$	$3d_{5/2}$		20	6.9	5, 6
$3d_{3/2}$	$3d_{5/2}$	−1.63		9.4	5, 6
$4s_{1/2}$	$4s_{1/2}$	−1.47	20		
$3d_{3/2}$	$4s_{1/2}$			14.1	5, 6
$2g_{7/2}$	$2g_{7/2}$	1.49	20	−31.3	5
$3d_{3/2}$	$2g_{7/2}$			−23.2	5, 6
$3d_{3/2}$	$3d_{3/2}$	1.12	20	−14.1	5

magnetic moment for the $\frac{1}{2}^+$ ground state of ^{205}Tl

$$\mu(^{205}\mathrm{Tl}) = 1.635 \pm 0.007 .$$

The ^{205}Tl ground state is, however, a three-hole state, containing collective admixtures which can be described by coupling single-hole components to the 2^+ first excited state in ^{206}Pb. These admixtures may cause a difference in the ^{205}Tl and ^{207}Tl ground state moments.

The authors acknowledge the contributions of Dr. H. J. Maier, who assisted in the fabrication of the targets, and of H. Steffens, who helped with the design and construction of the plunger chamber. Two of us (DJD and OH) acknowledge the hospitality extended to us at Sektion Physik der Universität München during our stay in Munich.

---

*On leave of absence from University of Arizona, Tucson, Arizona 85721.
†On leave of absence from Atomic Energy of Canada, Ltd., Chalk River, Ontario, Canada.

[1]A. Arima and L. J. Huang-Lin, Phys. Lett. B 41B, 429 (1972).
[2]R. Bauer, J. Speth, V. Klemb, P. Ring, E. Werner, and T. Yamazaki, Nucl. Phys. A A209, 535 (1973).
[3]F. C. Khanna and O. Häusser, Phys. Lett. B 45B, 12 (1973).
[4]J. Blomqvist, J. Phys. Soc. Jpn. 34, 223 (1973).
[5]P. Ring, R. Bauer, and J. Speth, Nucl. Phys. A A206, 97 (1973).
[6]O. Häusser, F. C. Khanna, and D. Ward, Nucl. Phys. A A194, 113 (1972).
[7]A. Olin, O. Häusser, D. Ward, and D. L. Disdier, Nucl. Phys. A A197, 583 (1972).
[8]T. T. S. Kuo and G. H. Herling, U. S. Naval Research Laboratory Report No. 2258, 1971 (unpublished); T. T. S. Kuo, Nucl. Phys. A A122, 325 (1968).
[9]C. W. Ma and W. W. True, Phys. Rev. C 8, 2313 (1973).
[10]T. K. Alexander and A. Bell, Nucl. Instrum. Methods 81, 22 (1970).
[11]K. H. Maier, K. Nakai, J. R. Leigh, R. M. Diamond, and F. S. Stephens, Nucl. Phys. A A186, 97 (1972).
[12]K. K. Seth, Nucl. Data B B7, 161 (1972).
[13]K. Nakai, B. Herskind, J. Blomqvist, A. Filevich, K. G. Rensfelt, J. Szarkier, and S. Nagamiya, Nucl. Phys. A A189, 526 (1972).
[14]H. Hübel, G. Günther, K. Euler, N. Bräner, and D. Riegel, Nucl. Phys. A A227, 421 (1974).
[15]K. Nagamine, H. Koyama, N. Nishida, M. Takizawa, K. Nakai, and T. Yamazaki, J. Phys. Soc. Jpn. Suppl. 34, 113 (1973).
[16]C. V. K. Baba, T. Faestermann, D. B. Fossan, and D. Proetel, Phys. Rev. Lett. 29, 496 (1972).
[17]C. V. K. Baba, D. B. Fossan, T. Faestermann, F. v. Feilitzsch, P. Kienle, and C. Signorini, Phys. Lett. B 43B, 483 (1973).
[18]A. Olin, O. Häusser, T. K. Alexander, A. J. Ferguson, and W. Witthuhn, Nucl. Phys. A A221, 555 (1974); private communication.
[19]M. B. Lewis, Nucl. Data B B5, 631 (1971).
[20]R. Bauer, J. Speth, V. Klemt, P. Ring, E. Werner, and T. Yamazaki, Nucl. Phys. A A209, 535 (1973).
[21]A. P. Komar *et al.*, Dokl. Akad. Nauk. SSSR 191, 61 (1970) [Sov. Phys.—Dokl. 15, 244 (1970)].
[22]M. J. Martin, Nucl. Data B B5, 287 (1971).
[23]S. Nagamiya, J. Phys. Soc. Jpn. 34, 623 (1973).
[24]O. Häusser, A. Olin, D. Ward, and W. Witthuhn, Phys. Lett. B 45B, 247 (1973).
[25]O. Häusser, D. B. Fossan, A. Olin, D. Ward, W. Witthuhn, and R. E. Warner, Nucl. Phys. A A225, 425 (1974).
[26]P. Salling, Phys. Lett. 17, 139 (1965).
[27]C. Ellegaard, P. D. Barnes, R. Eisenstein, and T. R. Canada, Phys. Lett. B 35B, 145 (1971); see also D. Proetel *et al.*, Phys. Rev. C 7, 2137 (1973).
[28]K. Nakai, B. Herskind, J. Blomqvist, A. Filevich, K.-G. Rensfelt, J. Starker, and S. Nagamiya, Nucl. Phys. A183, 526 (1972).
[29]W. W. True and K. W. Ford, Phys. Rev. 109, 1675 (1958).
[30]D. Proetel, M. Dost, E. Grosse, H. J. Körner, and P. Von Brentano, Nucl. Phys. A A161, 565 (1971).
[31]D. Proetel, F. Riess, E. Grosse, R. Ley, M. R. Maier, and P. Von Brentano, Phys. Rev. C 7, 2137 (1973).